nature catalysis

SUPPLEMENTARY INFORMATION

https://doi.org/10.1038/s41929-019-0279-6

In the format provided by the authors and unedited.

Single-atom tailoring of platinum nanocatalysts for high-performance multifunctional electrocatalysis

Mufan Li[1,2,12], Kaining Duanmu[3,12], Chengzhang Wan[1,12], Tao Cheng[4,5,12], Liang Zhang[6], Sheng Dai[7], Wenxin Chen[8], Zipeng Zhao[2], Peng Li[1], Huilong Fei[1], Yuanming Zhu[9], Rong Yu[9], Jun Luo[10], Ketao Zang[10], Zhaoyang Lin[1], Mengning Ding[2], Jin Huang[2], Hongtao Sun[1], Jinghua Guo[6], Xiaoqing Pan[7,11], William A. Goddard III[4], Philippe Sautet[1,3]*, Yu Huang[2]* and Xiangfeng Duan[1]*

[1]Department of Chemistry and Biochemistry, University of California, Los Angeles, CA, USA. [2]Department of Materials Science and Engineering, University of California, Los Angeles, CA, USA. [3]Department of Chemical and Biomolecular Engineering, University of California, Los Angeles, CA, USA. [4]Materials and Process Simulation Center, California Institute of Technology, Pasadena, CA, USA. [5]Institute of Functional Nano & Soft Materials (FUNSOM), Jiangsu Key Laboratory for Carbon-Based Functional Materials & Devices, Joint International Research Laboratory of Carbon-Based Functional Materials and Devices, Soochow University, Suzhou, Jiangsu, China. [6]Advanced Light Source, Lawrence Berkeley National Laboratory, Berkeley, CA, USA. [7]Department of Materials Science and Engineering, University of California Irvine, Irvine, CA, USA. [8]Department of Chemistry, Tsinghua University, Beijing, China. [9]National Center for Electron Microscopy in Beijing, School of Materials Science and Engineering, Tsinghua University, Beijing, China. [10]Center for Electron Microscopy in Tianjin University of Technology, Tianjin, China. [11]Irvine Materials Research Institute (IMRI), University of California Irvine, Irvine, CA, USA. [12]These authors contributed equally: Mufan Li, Kaining Duanmu, Chengzhang Wan, Tao Cheng. *e-mail: sautet@ucla.edu; yhuang@seas.ucla.edu; xduan@chem.ucla.edu

Supplymentary Information for

Single-atom tailoring of platinum nanocatalysts for high-performance multifunctional electrocatalysis

Mufan Li[1,2,13], Kaining Duanmu[3,13], Chengzhang Wan[1,13], Tao Cheng[4,5,13], Liang Zhang[6], Sheng Dai[7], Wenxin Chen[8], Zipeng Zhao[2], Peng Li[1], Huilong Fei[1], Yuanming Zhu[9], Rong Yu[9], Jun Luo[10], Ketao Zang[10], Zhaoyang Lin[1], Mengning Ding[2], Jin Huang[2], Hongtao Sun[1], Jinghua Guo[6], Xiaoqing Pan[7,11], William A. Goddard III[4], Philippe Sautet[1,3,12], Yu Huang[2,12*], Xiangfeng Duan[1,12*]*

[1]Department of Chemistry and Biochemistry, University of California, Los Angeles, Los Angeles, California 90095, USA; [2]Department of Materials Science and Engineering, University of California, Los Angeles, CA 90095, USA; [3]Department of Chemical and Biomolecular Engineering, University of California, Los Angeles, CA 90095, USA; [4]Materials and Process Simulation Center, California Institute of Technology, Pasadena, CA 91125, USA; [5]Institute of Functional Nano & Soft Materials (FUNSOM), Jiangsu Key Laboratory for Carbon-Based Functional Materials & Devices, Joint International Research Laboratory of Carbon-Based Functional Materials and Devices, Soochow University, Suzhou, Jiangsu, 215123, P. R. China; [6]Advanced Light Source, Lawrence Berkeley National Laboratory, Berkeley, CA 94720, *USA*; [7]Department of Materials Science and Engineering, University of California Irvine, Irvine, California 92697, USA; [8]Departmentof Chemistry, Tsinghua University, Beijing 100084, P. R. China; [9]National Center for Electron Microscopy in Beijing, School of Materials Science and Engineering, Tsinghua University, Beijing 100084, P. R. China; [10]Center for Electron Microscopy in Tianjin University of Technology, Tianjin 300384, P. R. China; [11]Irvine Materials Research Institute (IMRI), University of California Irvine, Irvine, California 92697, USA; [12]California NanoSystems Institute, University of California, Los Angeles, Los Angeles, California 90095, USA. [13]These authors contributed equally to this work.

[*]Correspondence to: xduan@chem.ucla.edu, yhuang@seas.ucla.edu, sautet@ucla.edu

This PDF file includes:

Supplementary Figures 1 to 11

Supplementary Tables 1 to 4

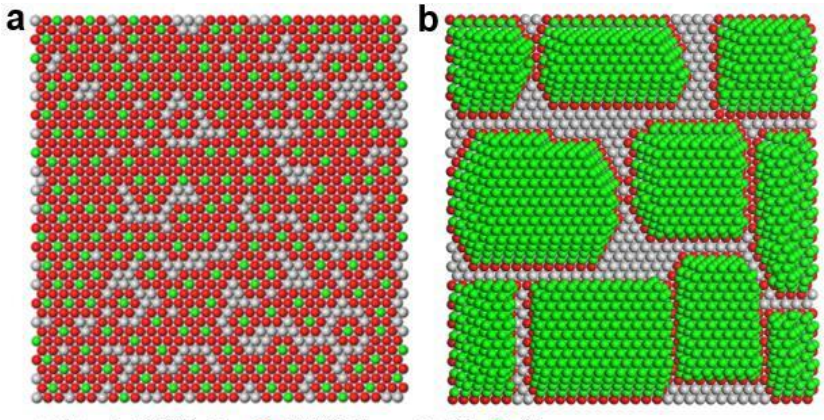

c

	Surface Pt sites before decoration	Surface Pt sites after decoration	Pt sites with Ni neighbor	Pt sites w/o Ni neighbor	Pt sites blocked by Ni
SANi decorated Pt surface	1394	1204	933	271	190
Ni NPs decorated Pt surface	1394	557	356	201	837

Supplementary Fig. 1 | A simplified model of Pt (111) surface decorated by (**a**) single Ni atom species [*$Ni(OH)_2$ species, simplified as Ni*] and (**b**) 1-2 nm nanoparticles, with grey representing regular Pt (111) surface site, red representing activated Pt atoms with Ni neighbor, and green representing sites blocked by Ni. (**c**) Comparing different types of Pt sites for the single atom and nanoparticle decorated Pt surface in the simplified model in a and b. For a Pt (111) surface with a total 1394 Pt sites decorated with 190 single Ni atoms (green), there are a total of 1204 exposed Pt atoms, with 933 having a Ni neighbor (red) and 271 having no Ni neighbor (blue); while for the same Pt (111) surface (a total of 1394 initial Pt surface sites) decorated with 1-2 nm Ni nanoparticles, there are only 557 exposed Pt atoms on surface, with 356 having a Ni neighbor and 201 without Ni neighbor. This comparison highlights the single atom modifications activate a lot more surface sites (with Ni neighbors) while blocking much fewer Pt sites.

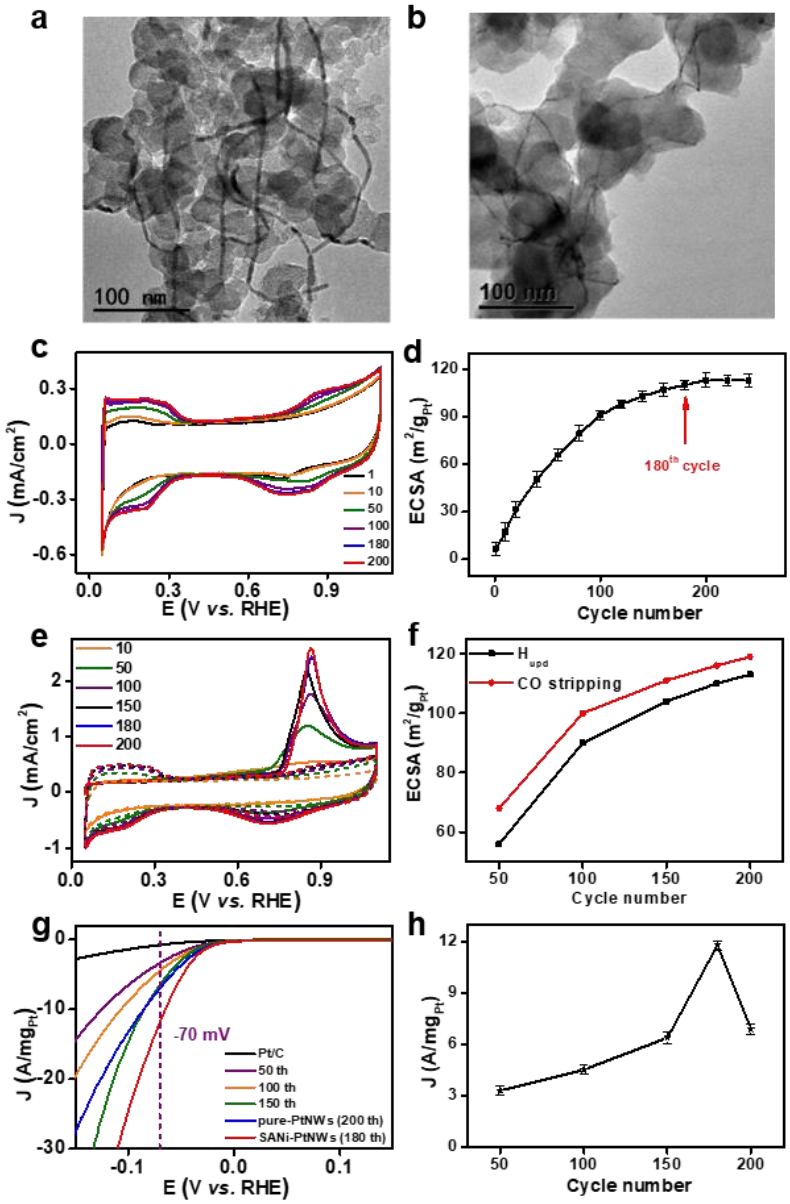

Supplementary Fig. 2 | (**a**) TEM images of PtNi alloy nanowire and (**b**) TEM images of SANi-PtNWs. (**c**) CV in 0.1 M $HClO_4$ of PtNi alloy NWs at different scan cycles. (**d**) ECSA evolution of the nanowire samples with increasing number of dealloying CV cycles (error bars showing the variations from ten independent batches). (**e**) The acidic CO stripping curves for $Pt_{17}Ni_{83}$ nanowires de-alloyed at different cycles. (**f**) Comparison of the ECSA evolution (vs. the number of dealloying CV cycles) derived from Hupd and CO stripping, respectively. (**g**) HER polarization curve for Pt/C and PtNi nanowires dealloyed with different numbers of CV cycles. (**h**) The mass activity of the dealloyed nanowires as a function of the number CV cycles, with the peak HER activity achieved after the 180th CV cycles (error bars showing the variations from ten independent batches), when the surface decorating species is in single atomic state to ensure maximum activation and the least surface blockage.

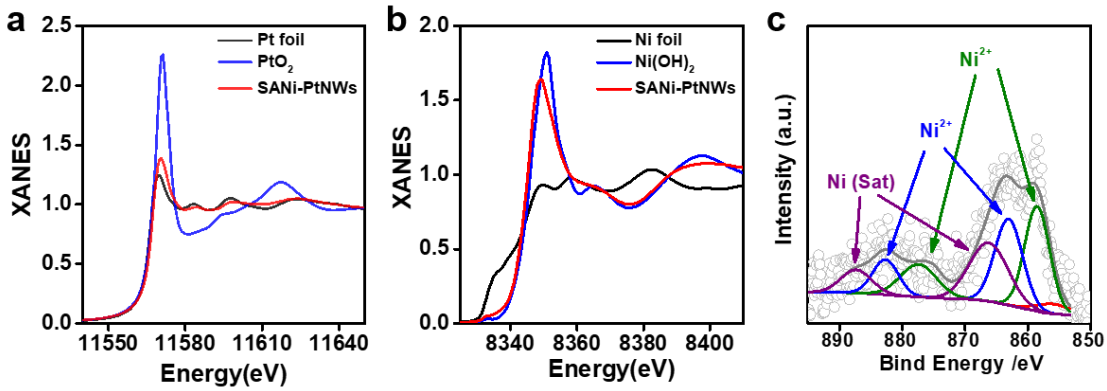

Supplementary Fig. 3 | (**a**) XANES spectra of Pt L_3-edge and (**b**) XANES spectra of Ni K-edge. (**c**) The XPS result for Ni 2p of SANi-PtNWs post electrocatalytic test.

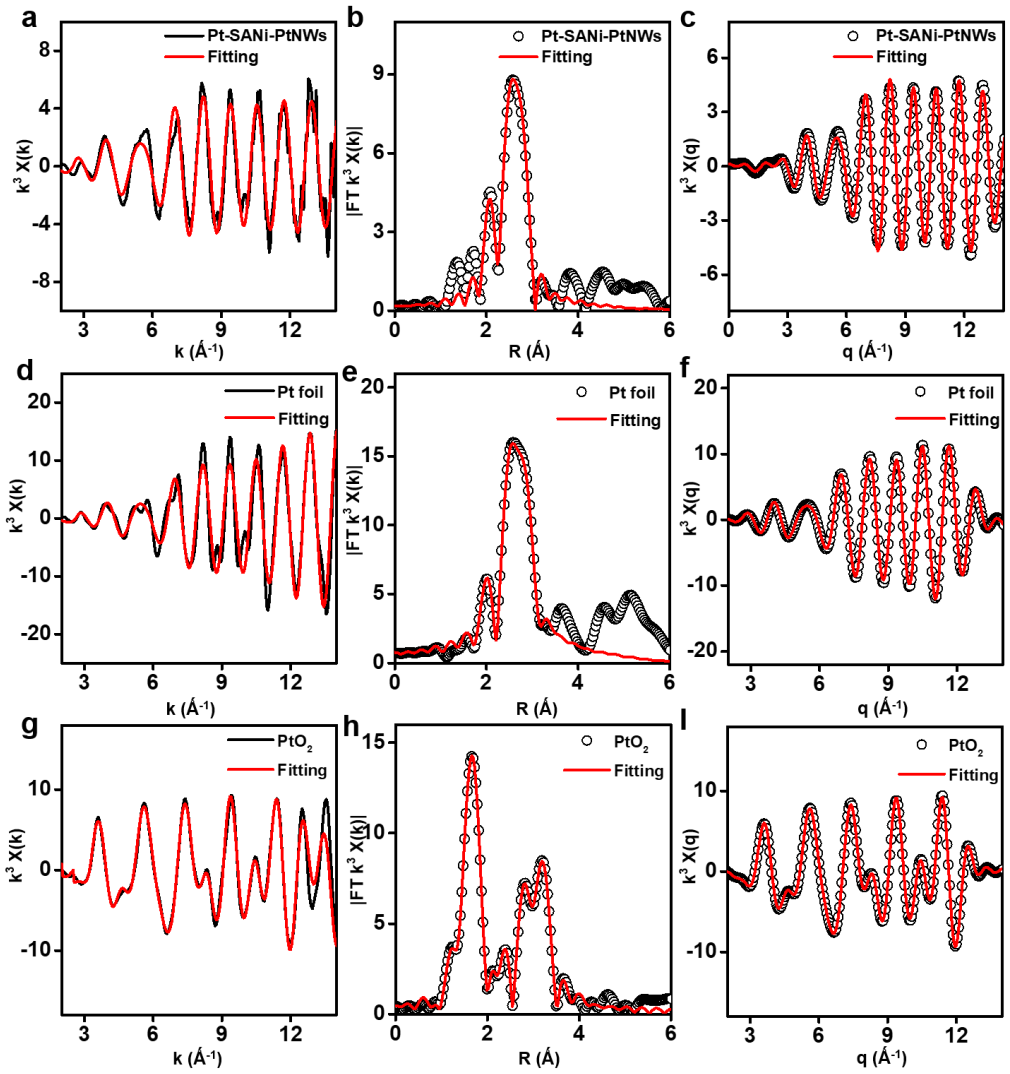

Supplementary Fig. 4 | Fitting results of SANi-PtNWs, Pt foil and PtO_2 at Pt L_3-edge. (**a**) (**d**) (**g**) The k space fitting curves. (**b**) (**e**) (**h**) The FT-EXAFS fitting curves. (FT range: 2-12.5 $Å^{-1}$; fitting range: 0.8-3.4 Å). (**c**) (**f**) (**i**) The inversed FT-EXAFS fitting curves.

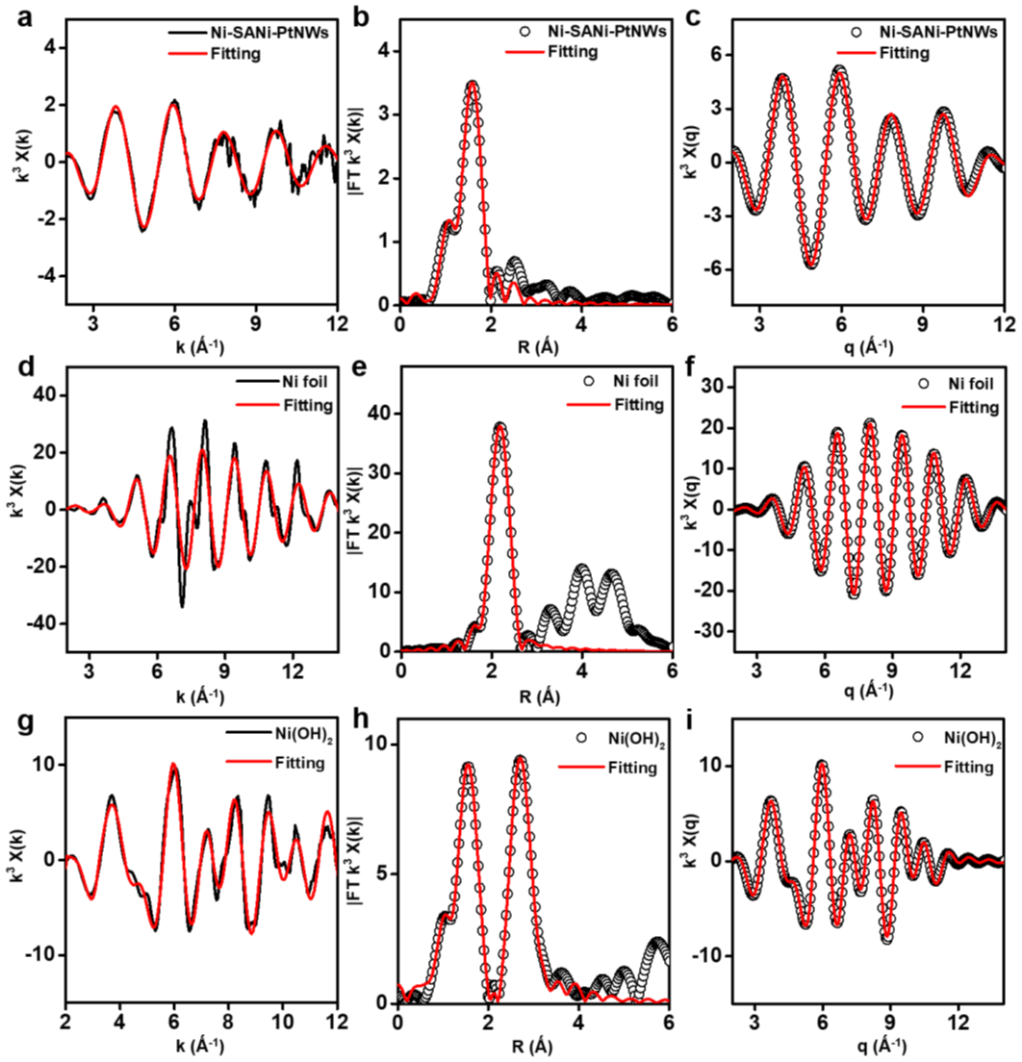

Supplementary Fig. 5 | Fitting results of SANi-PtNWs, Ni foil and $Ni(OH)_2$ at Ni k-edge. (**a**) (**d**) (**g**) The k space fitting curves. (**b**) (**e**) (**h**) The FT-EXAFS fitting curves (FT range: 2-12.5 $Å^{-1}$; fitting range: 0.8-3.4 Å). (**c**) (**f**) (**i**) The inversed FT-EXAFS fitting curves.

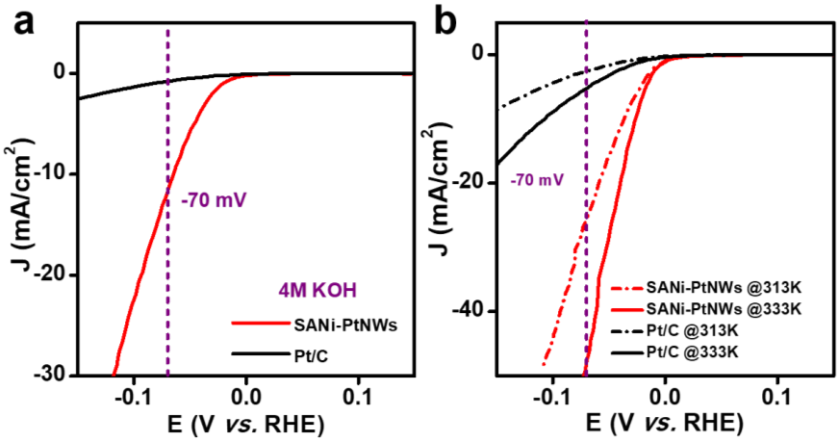

Supplementary Fig. 6 | HER performance of the SANi-PtNWs and Pt/C under harsher conditions. (**a**) ECSA normalized HER LSVs for Pt/C and SANi-PtNWs in 4 M KOH with 95% iR-compensation at the scan rate of 5 mV/s. (**b**) ECSA normalized HER LSVs for Pt/C and SANi-PtNWs at 313 K and 333 K, respectively. The measurements were conducted in 1 M KOH with 95% iR-compensation at the scan rate of 5 mV/s.

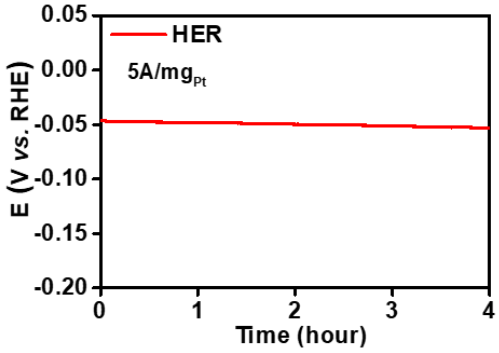

Supplementary Fig. 7 | HER chronopotentiometry test of SANi-PtNWs, in 1 M KOH at a constant current density of 5 A/mg$_{Pt}$.

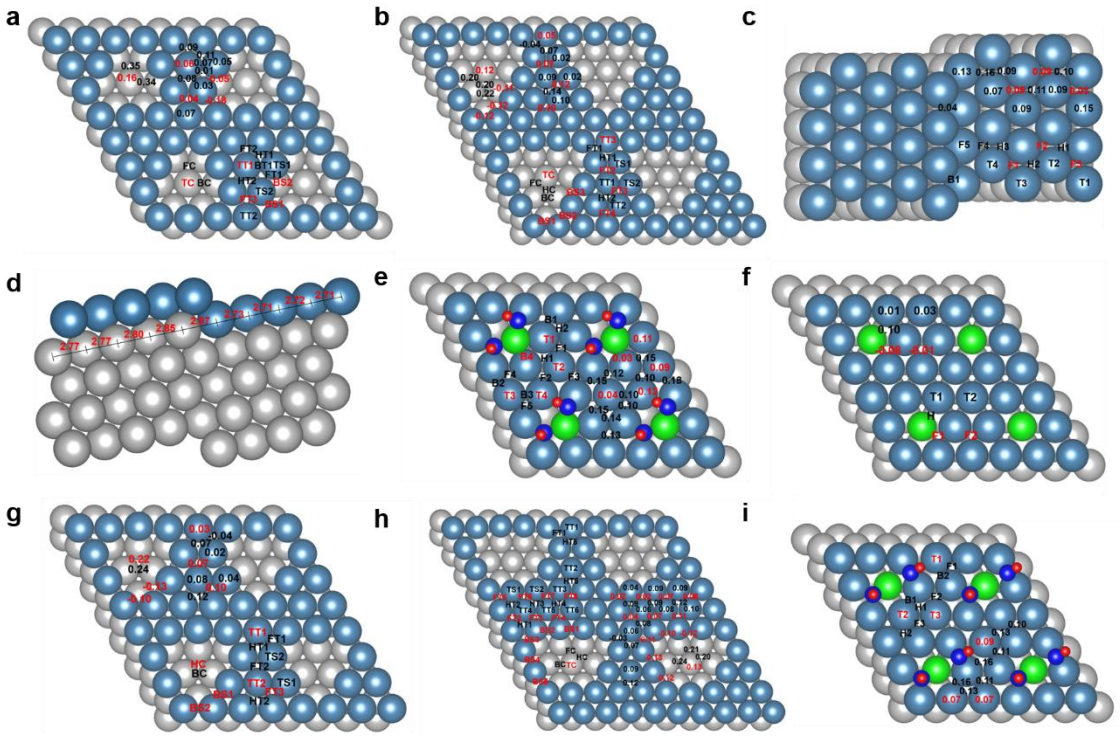

Supplementary Fig. 8 | DFT models for HER activity calculation. To better distinguish the sites in Models A, C, E, and F, we use two letters to label the adsorption sites. The first letter indicates whether the site is top (T), bridge (B), FCC hollow (F) or HCP hollow (H), the second letter indicates whether the site is in a cavity (C), on the step (S), or on the terrace (T). For the adsorption sites in Models B, D and G, there are no cavities so we use simple labels to represent whether the site is top (T), bridge (B), FCC hollow (F) or HCP hollow (H). The local minima sites are in red color. The adsorption free energies ($\Delta G_H - \Delta G_H^{Pt\,(111)}$) for all the adsorption sites are shown in Supplementary Table 3. Besides that, we also directly write the adsorption free energies on the adsorption sites. The local minima sites are in red color. (**a**) Model A with 4×4 unit cell and 5 layers. BS1 and BS2 are the most stable adsorption sites. By symmetry, there are 3 BS1 and 6 BS2 sites in one unit cell. Since they will be occupied first and they will block TS1, TS2 and FT1 sites, FT3 and TT1 sites will become the local minima sites. The TC site in the cavity is another local minimum. (**b**) Model B with 5×5 unit cell and 5 layers. Model C has a larger cavity than Model A, but there are many similarities. The BS sites are still the most stable sites. The TS sites have lower energies than TT3, FT2 and FT3, but they are blocked by the BS sites, so the local minima sites on the terrace are TT3, FT2, FT3 and FT4. The TC site in the cavity is still a local minimum site. (**c**) Model C of Pt (553) stepped surface. (**d**) Bond lengths (Å) in model C. The Pt-Pt distance in bulk is 2.81 Å. Model C is Pt (553) surface and it's a model for the step defect. We find the fcc hollow sites, such as F1, F2 and F3 are destabilized compared to Pt (111), which could be explained by the strain effect. In this figure, we can see that the bond lengths between the terrace atoms are about 3.5% less than the normal distance in the Pt bulk. (**e**) Model D with 3×3 unit cell and 5 layers. Model D is the (OH) bounded Ni single atoms decorated Pt (111) surface. B1 is the most preferred site, then T3, T2 and T1 sites will be covered if more H is adsorbed. Since all the other sites are blocked, T4 will be covered if one more H atom comes in although it's not a local minimum. If higher coverage

is reached, the fcc sites and B2 site rather than the top sites will be covered. (**f**) SANi/Pt model with 3×3 unit cell and 5 layers. This model has no OH groups binding to the Ni, the fcc hollow sites F1 and F2 are the locally stable sites, and they are less active than Pt (111). (**g**) Model E with 4×4 unit cell and 5 layers. This is another model of Pt (111) with a cavity. (**h**) Model F with 5×5 unit cell and 5 layers. This is another model of Pt (111) with a cavity. (**i**) Model G with 3×3 unit cell and 5 layers. Model G is an isomer of model D, which is also (OH) bounded SANi decorated Pt (111) surface, it's 0.027 eV higher in energy. All the sites on this model are also more active than Pt (111).

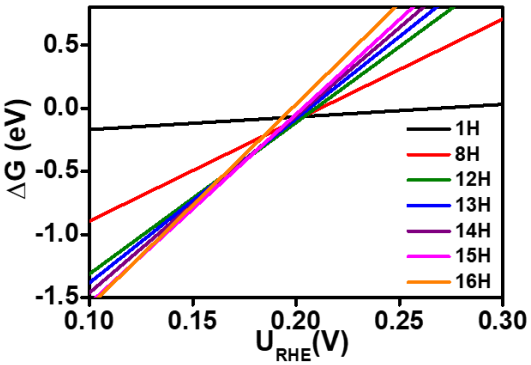

Supplementary Fig. 9 | Adsorption free energy of hydrogen on a 4×4 unit cell of Pt (111) surface as a function of U_{RHE} at various coverage in pH=14 solution. This figure shows that in experimental condition of -70 mV *vs.* RHE, the Pt (111) surface adsorbs 1 monolayer of H.

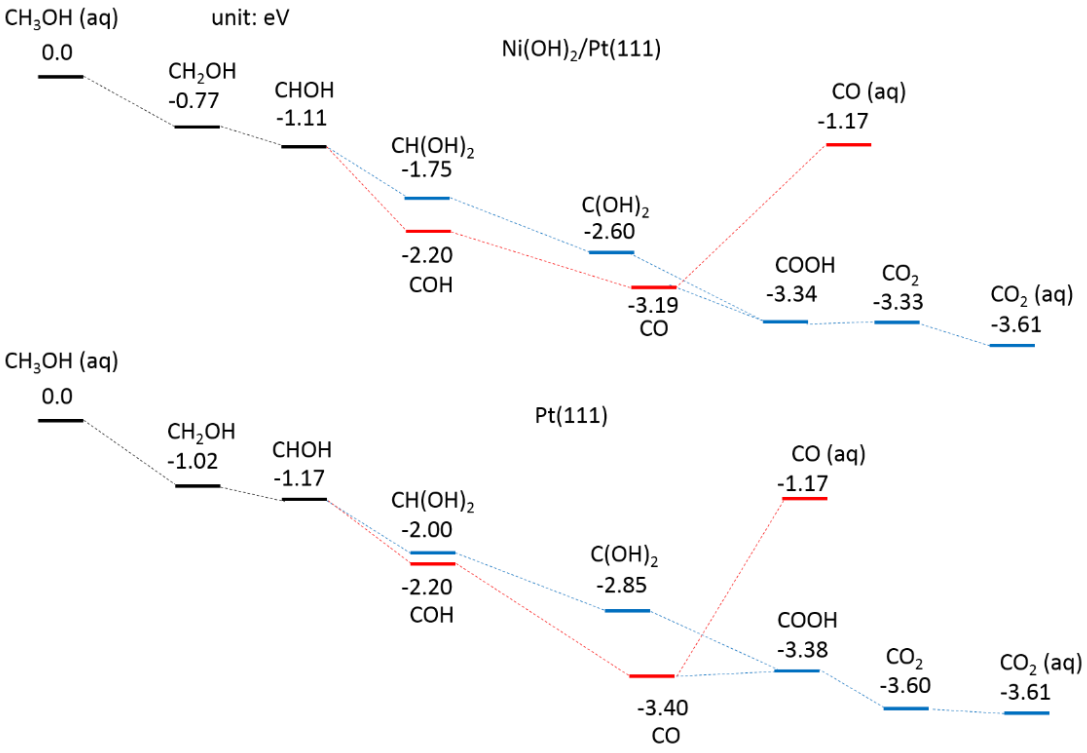

Supplementary Fig. 10 | Reaction profile for MOR on $Ni(OH)_2/Pt(111)$ (top) and Pt(111) (bottom). A continuum solvent model with dielectric constant 78.4 was used, together with a potential of 0.65 V *vs.* RHE.

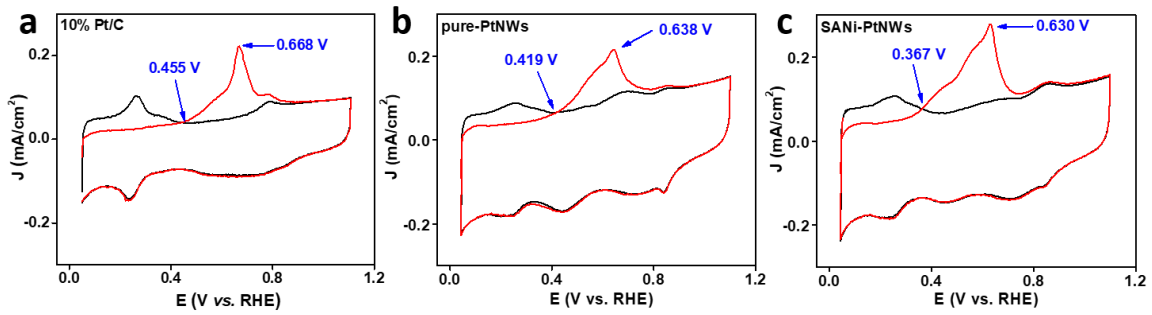

Supplementary Fig. 11 | The CO stripping results for (**a**) 10% Pt/C, (**b**) pure-PtNWs, and (**c**) SANi-PtNWs. The measurements were conducted in 1 M KOH at the scan rate of 25 mV/s.

Supplementary Table 1 | Structural parameters extracted from the Pt L_3-edge EXAFS fitting. (S_0^2=0.78)

Sample	Scattering pair	CN	R(Å)	$\sigma^2(10^{-3}Å^2)$	ΔE_0(eV)	R factor
SANi-PtNWs	Pt-Pt	8.9	2.74	7.1	5.4	0.01
Pt foil	Pt-Pt	12*	2.79	4.3	7.7	0.0062
PtO_2 bulk	Pt-O	2*	1.97	3.2	7.5	0.0043
	Pt-O	4*	2.05	4.1		
	Pt-Pt	2*	3.12	3.4	13.6	

S_0^2 is the amplitude reduction factor; CN is the coordination number; R is interatomic distance (the bond length between Pt central atoms and surrounding coordination atoms); σ^2 is Debye-Waller factor (a measure of thermal and static disorder in absorber-scatterer distances); ΔE_0 is edge-energy shift (the difference between the zero kinetic energy value of the sample and that of the theoretical model). R factor is used to value the goodness of the fitting. * This value was fixed during EXAFS fitting, based on the known structure of Pt metal and PtO_2 bulk.

Error bounds that characterize the structural parameters obtained by EXAFS spectroscopy were estimated as N ± 20%; R ± 1%; σ^2 ± 20%; ΔE_0 ± 20%.

Supplementary Table 2 | Structural parameters extracted from the Ni K-edge EXAFS fitting (S_0^2=0.77).

Sample	Scattering pair	CN	R(Å)	$\sigma^2(10^{-3}Å^2)$	ΔE_0(eV)	R factor
SANi-PtNWs	Ni-O	2.3	2.04	5.3	-2.5	0.01
Ni foil	Ni-Ni	12*	2.49	5.9	6.1	0.0013
$Ni(OH)_2$ bulk	Ni-O	6*	2.05	5.3	4.3	0.0038
	Ni-Ni	6*	3.12	6.4	7.2	

S_0^2 is the amplitude reduction factor; CN is the coordination number; R is interatomic distance (the bond length between Ni central atoms and surrounding coordination atoms); σ^2 is Debye-Waller factor (a measure of thermal and static disorder in absorber-scatterer distances); ΔE_0 is edge-energy shift (the difference between the zero kinetic energy value of the sample and that of the theoretical model). R factor is used to value the goodness of the fitting. * This value was fixed during EXAFS fitting, based on the known structure of Ni metal and $Ni(OH)_2$ bulk.

Error bounds that characterize the structural parameters obtained by EXAFS spectroscopy were estimated as N ± 20%; R ± 1%; σ^2 ± 20%; ΔE_0 ± 20%.

Supplementary Table 3 | Adsorption Free Energies for Adsorption Sites in Models A-G (unit: eV).[‡]

model A	ΔΔG	model B	ΔΔG	model C	ΔΔG	model F	ΔΔG
BC	0.341	BC	0.218	B1	0.044	BC	0.235
BS1	-0.180	BS1	-0.118	F1	0.049	BS1	-0.121
BS2	-0.047	BS2	-0.123	F2	0.089	BS2	-0.104
BT1	0.077	BS3	-0.109	F3	0.033	BS3	-0.110
FC	0.349	FC	0.197	F4	0.163	BS4	-0.134
FT1	0.011	FT1	-0.039	F5	0.131	BS5	-0.117
FT2	0.088	FT2	0.066	H1	0.100	FC	0.205
FT3	0.039	FT3	0.115	H2	0.108	FT1	-0.028
HT1	0.105	FT4	0.099	H3	0.087	FT2	0.040
HT2	0.081	HC	0.199	T1	0.151	FT3	0.072
TC	0.161	HT1	0.071	T2	0.087	FT4	0.114
TS1	0.049	HT2	0.137	T3	0.090	FT5	0.017
TS2	0.024	TC	0.116	T4	0.069	FT6	0.017
TT1	0.055	TS1	0.023			FT7	0.073
TT2	0.066	TS2	0.022			FT8	0.082
		TT1	0.088			HC	0.198
		TT2	0.100			HT1	0.075
		TT3	0.049			HT2	0.090
						HT3	0.088
model D	ΔΔG	model E	ΔΔG	model G	ΔΔG	HT4	0.118
B1	0.030	BC	0.241	B1	0.156	HT5	0.123
B2	0.145	BS1	-0.127	B2	0.156	HT6	0.068
B3	0.148	BS2	-0.104	F1	0.111	TC	0.126
B4	0.098	FT1	-0.039	F2	0.112	TS1	0.042
F1	0.127	FT2	0.070	F3	0.096	TS2	0.085
F2	0.097	FT3	0.101	H1	0.126	TT1	0.059
F3	0.175	HC	0.218	H2	0.134	TT2	0.086
F4	0.120	HT1	0.068	T1	0.091	TT3	0.091
F5	0.100	HT2	0.118	T2	0.072	TT4	0.061
H1	0.146	TS1	0.035	T3	0.071	TT5	0.083
H2	0.142	TS2	0.020			TT6	0.103
T1	0.108	TT1	0.033				
T2	0.087	TT2	0.080				
T3	0.042						
T4	0.120						

[‡]The adsorption free energy is expressed in $\Delta G_H - \Delta G_H^{Pt\,(111)}$ (ΔΔG), which is the difference between the actual free energy ΔG_H and the adsorption free energy on Pt (111) surface $\Delta G_H^{Pt\,(111)}$.

Supplementary Table 4 | CO adsorption energies for adsorption sites shown in Fig. 5f.

Adsorption site	ΔE/eV
Pt (111)	-1.77
T1	-1.54
T2	-1.64
T3	-1.71
T4	-1.69